PRIMERS IN MICROSCOPY

Removal of hydrocarbon contamination and oxide films from atom probe specimens

Michael Herbig ⓘ | Ankit Kumar

Department of Microstructure Physics and Alloy Design, Max-Planck-Institut für Eisenforschung GmbH, Düsseldorf, Germany

Correspondence
Michael Herbig, Max-Planck-Institut für Eisenforschung GmbH, Max-Planck-Str. 1, 40237 Düsseldorf, Germany.
Email: m.herbig@mpie.de, herbig.michael@gmail.com

Abstract

Many materials science phenomena require joint structural and chemical characterization at the nanometer scale to be understood. This can be achieved by correlating electron microscopy (EM) and atom probe tomography (APT) subsequently on the same specimen. For this approach, specimen yield during APT is of particular importance, as significantly more instrument time per specimen is invested as compared to conventional APT measurements. However, electron microscopy causes hydrocarbon contamination on the surface of atom probe specimens. Also, oxide layers grow during specimen transport between instruments and storage. Both effects lower the chances for long and smooth runs in the ensuing APT experiment. This represents a crucial bottleneck of the method correlative EM/APT. Here, we present a simple and reliable method based on argon ion polishing that is able to remove hydrocarbon contamination and oxide layers, thereby significantly improving APT specimen yield, particularly after EM.

KEYWORDS
atom probe tomography (APT), correlative EM/APT, hydrocarbon contamination, scanning electron microscopy (SEM), transmission electron microscopy (TEM)

1 | INTRODUCTION

Materials science inherently involves combined structural and compositional changes at the atomistic scale. Understanding the origin of many macroscopic phenomena requires accessing this combined information and length scale. This can be achieved by the joint use of electron microscopy (EM) for structural characterization and atom probe tomography (APT) for compositional analysis at the same location (correlative EM/APT) (Felfer, Alam, Ringer, & Cairney, 2012; Herbig, 2018; Herbig, Choi, & Raabe, 2015), a method which evolved from early approaches correlating EM and field ion microscopy (FIM) (Krakauer et al., 1990; Loberg & Norden, 1969). Correlative EM/APT is a key technique that enables investigating correlations between the crystallographic character of defects (e.g., grain boundaries, stacking faults, dislocations) and solute segregation (Herbig et al., 2014;

Herbig, Kuzmina, et al., 2015; Liebscher et al., 2018; Stoffers et al., 2015; Zhou, Yu, Kaub, Martens, & Thompson, 2016), correlations between optical properties and composition (Rigutti et al., 2014), the investigation of local phase transformations (Kuzmina, Herbig, Ponge, Sandlobes, & Raabe, 2015; Toji, Matsuda, Herbig, Choi, & Raabe, 2014), or the fine tuning of atom probe reconstruction parameters (Haley, Petersen, Ringer, & Smith, 2011). This technique is conducted on conical specimens with tip radii of about 20–50 nm and half shank angles in the order of 10°. This geometry ensures electron transparency for the top 200 nm of the specimens in a 200 kV electron beam even for high electron density materials such as steels. The conical geometry is needed to conduct APT. It locally amplifies the electric field applied during APT measurements to the specimens at the tip apex to an extent where atomic bonds are broken. Individual atoms then become ionized and accelerated towards a 2D detection system.

The ion type is identified based on the time of flight. In combination with the sequence of arrival of the ion and its position of arrival on the detection system the former atomic built-up of the specimen is reconstructed in 3D. The bottleneck of the powerful method correlative EM/APT is that EM investigations significantly reduce the measurement yield in the subsequent APT experiments. The specimens fail significantly earlier as compared to the ones measured by APT directly after specimen preparation, either by fracture or by melting caused by electric discharge events. Correlative EM/APT of selected regions of interest (ROIs), such as particular grain boundaries, usually requires target preparation of the ROI into the specimen apex. This involves iterative localization of the ROI by EM and milling of the specimen by a focused ion beam (FIB). Due to the high experimental efforts involved in this target preparation routine, specimen failure during the ensuing APT experiment before the ROI was successfully measured represents a major loss. The same holds for correlative EM/APT experiments involving complex TEM analysis, such as the characterization of the dislocation character. Thus, correlative EM/APT requires dedicating significantly more experimental time and effort to each specimen as compared to conventional APT runs but at the same time the chances for a successful APT experiment are reduced. And without successful ensuing APT experiment, the prior EM experiment is practically worthless, as EM can be conducted in easier and statistically more robust way on conventional EM specimens.

Further, prior EM investigations do not only reduce the APT measurement yield but can also deteriorate the quality of the APT measurement. Good APT experiments are characterized by a steadily increasing voltage applied between specimen and local electrode and a constant ion detection rate. For specimens pre-characterized by

EM, often sudden bursts of evaporation events or microfracture events are observed, even for materials that usually show smooth voltage curves. A microfracture event means that the top part of the specimen breaks off which bluntens the tip. This shows up as a sudden increase in voltage as the system regulates the number of ions detected per time to a specific target evaporation rate. The corresponding specimen part is missing in the reconstructed 3D atom map. Figure 1 illustrates this situation. These experiments, as well as all other experimental data shown in this work, were conducted on high carbon steels. The curves depicted in Figure 1b are representative for steels measured by APT after EM. A similar behavior is observed for most other materials classes.

The negative effects of EM on APT specimen yield and measurement quality are caused by hydrocarbon contamination and oxide layers on the specimen. On the one hand, the poor electric conductivity of these detrimental layers impedes the transport of electrons through the specimens that is required to ionize the atoms during APT which is particularly an issue for fast voltage pulses (Gault, Menand, de Geuser, Deconihout, & Danoix, 2006). On the other hand, these detrimental layers tend to field evaporate as larger fragments and in cascades due to poor cohesion with the original specimen surface, thereby causing bursts of events. These can oversaturate the detector, or generate conductive ion channels between specimen and local electrode that can trigger electric discharge events melting the specimen.

Conventional APT specimens are measured directly after preparation. Only little oxidation can occur while the specimens are exposed to air between preparation and APT measurement. Correlative EM/APT measurements require at least one additional exposure of the specimen to air during transport between the instruments. Also,
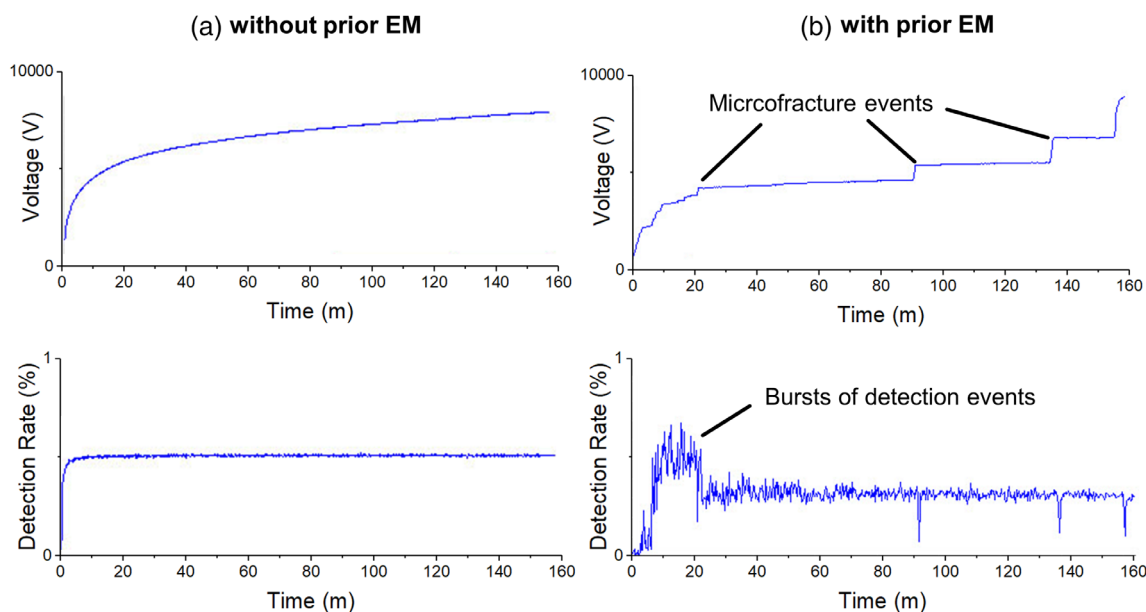

FIGURE 1 Effect of EM on APT measurement quality. (a) When directly measuring the specimen after preparation a smooth evolution of voltage and detection rate over time is observed. (b) The same material measured using the same APT parameters shows microfractures and bursts of detection events when being pre-characterized by EM [Color figure can be viewed at wileyonlinelibrary.com]

correlative EM/APT measurements often involve waiting times for an EM measurement time slot during which specimens slightly oxidize, even if they are stored under vacuum. Hydrocarbon contamination is generated by EM. For reasons of simplicity and efficiency EM is usually conducted in a scanning electron microscope (SEM) when spatial resolutions above ~6 nm are sufficient. The most frequently used EM technique on APT specimens is transmission Kikuchi diffraction (TKD) (Babinsky, De Kloe, Clemens, & Primig, 2014). In all other cases EM characterization must be conducted in the TEM. Either way, both cases of EM lead to hydrocarbon contamination on the specimen surface. Small hydrocarbon molecules deposit during exposure to air or due to poor vacuum conditions in the instrument on specimens and sample holder. These have high surface diffusion rates even at room temperature due to their small size, also under vacuum conditions present in electron microscopes. The interaction with an electron beam causes polymerization of these molecules to larger, immobile hydrocarbon compounds (Hettler et al., 2017; Love, Scott, Dennis, & Laurenson, 1981). The longer an area is investigated by EM, and the dirtier the specimen and sample holder surface or the measurement chamber, the thicker will be the hydrocarbon contamination. In EM these layers are known to limit the quantification of the element carbon and to cause scanning artefacts. Due to their poor electric conductivity, the incident electrons only slowly dissipate into the surrounding. Local surface charges accumulate in the investigated area which repel the incident electron beam. Examples of detrimental surface layers on APT specimens are depicted in Figure 2. In the TEM, the hydrocarbon contamination grows primarily on top and on bottom of the specimen, in direction of the incident beam and is thus often overlooked. However, when tilting the specimen after an extended TEM scan to 90° the hydrocarbon contamination becomes clearly visible (Figure 2a).

Figure 2b shows a specimen after a TKD scan in the SEM. Due to the low acceleration voltage used in the SEM only a small fraction of the beam is transmitted and thus the hydrocarbon contamination is mainly found at the top of the specimen. The low acceleration voltage used in SEMs causes that the beam interacts more efficiently with organic compounds. Further, SEMs are usually less clean than TEMs and operate under weaker vacuum conditions. Therefore, hydrocarbon contamination usually builds up even faster in the SEM than in the TEM. Imaging of the specimen tips at higher magnifications reveals that not only hydrocarbon contamination is present on the surface but additionally oxide layers (Figure 3a).

Hydrocarbon contamination during EM can be efficiently prevented by plasma cleaning of the specimen before the experiment. By igniting a plasma in an oxygen atmosphere, oxygen ions and radicals are generated that react with the hydrocarbon species on the surface to gaseous compounds which are then removed by the vacuum (Isabell, Fischione, O'Keefe, Guruz, & Dravid, 1999). However, as the method works with oxygen it will also oxidize the specimens. It thus can only be applied to remove hydrocarbon contamination but not to remove oxide layers. This issue is shown in Figure 3: after plasma cleaning the hydrocarbon contamination has vanished but not the additionally present oxide layer.

Today, the standard method to remove oxide layers and hydrocarbon contamination from APT specimens is low kV-FIB milling (Thompson, Gorman, Larson, Leer, & Hong, 2006). The specimen is pointed directly into the ion source in a SEM/FIB cross-beam instrument and then bombarded by gallium ions from the top at acceleration voltages of about 2–5 kV. Using low acceleration voltages prevents beam damage but impedes focusing the beam. The beam is targeted in a hardly controllable way to the entire specimen apex. SEM and TEM images of specimens cleaned in this way are shown in Figure 4. The procedure removes significantly more material from the specimen top than from the sides. At the specimen apex, not only the detrimental layers but also large parts of the specimen itself are removed whereas the detrimental layers at the specimen shank remain. Although this procedure improves specimen yield, it is not improved to an extent that could be compared to specimens that have not been exposed to EM, most likely due to the remaining contamination at the specimen shank. Further, the method has several disadvantages: The material loss at the specimen apex removes the thinnest specimen parts. This is the only part of the specimen where high
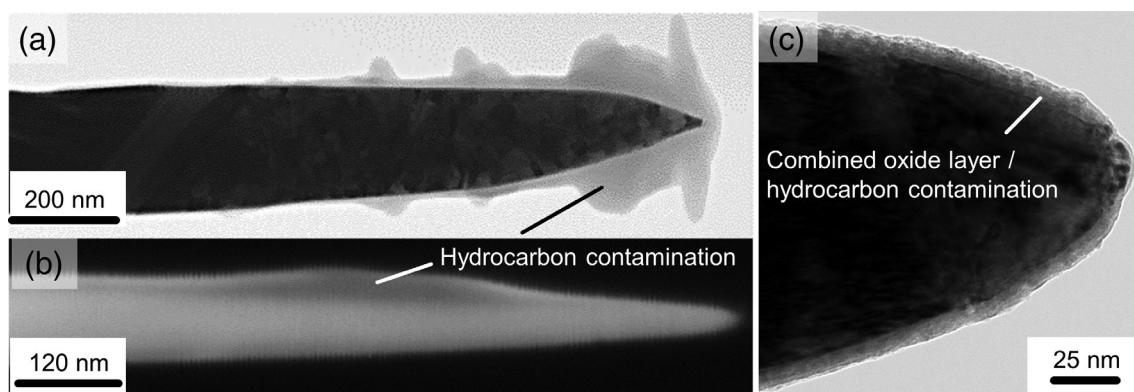

FIGURE 2 Detrimental surface layers on APT specimens. Hydrocarbon contamination created in a 200 kV TEM (a) and a 30 kV SEM (b). Combined oxide layer/hydrocarbon contamination created by the combination of specimen transport in air and a TEM measurement (c). A magnified view of (c) is shown in Figure 3a
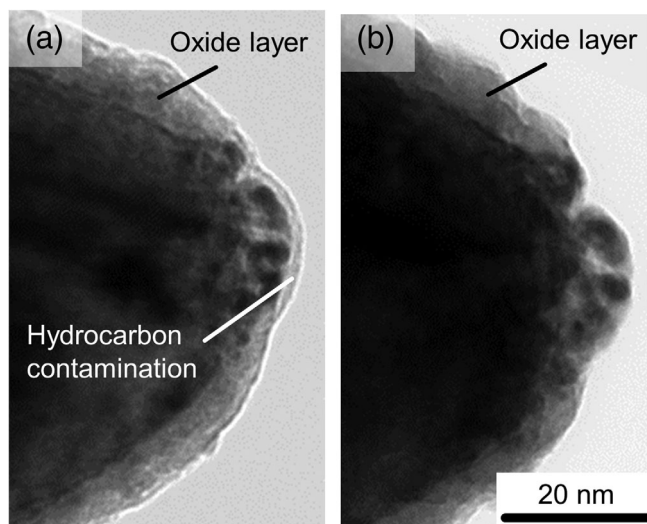
FIGURE 3 TEM micrographs showing an APT specimen apex. (a) Magnification of Figure 2c. After specimen transport in air and TEM investigation a combination of oxide layer and hydrocarbon contamination has formed on the surface. (b) Same specimen after 12 hours of plasma cleaning in air. While this method can remove hydrocarbon contamination it is unable to remove oxide layers
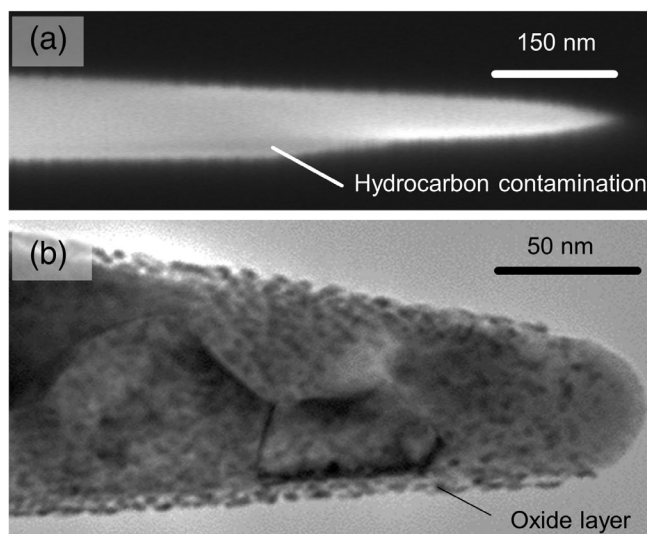

FIGURE 4 Specimens cleaned after EM by low kV FIB milling from the top. This procedure only removes contamination and oxide layers from the top, not from the sides. (a) SEM image. (b) TEM image

resolution—TEM can be performed and in general the location where the highest EM characterization quality can be achieved. Moreover, specimen drift during FIB milling causes that the material removal at the sample apex can hardly be quantified. Thus, there is a risk of removing the ROI investigated by EM in this step. Also, the method involves processing the specimens in a costly cross-beam SEM/FIB one by one what makes the technique costly and time-consuming.

In the following we present a technique that removes such layers after EM in a fast, reliable and easily applicable way, thereby rendering

correlative EM/APT more efficient and making this important technique more applicable in particular for cases that involve target preparation of an ROI or complex TEM experiments. For cleaning we employ a precision etching and coating system (PECS) which is normally used for polishing, etching and coating the surface of mm-sized SEM samples prior to EM.

2 | EXPERIMENTAL DETAILS

All experiments were conducted on high carbon steel. The specimens were prepared on halved molybdenum grids held in grid holders (Herbig, Choi, & Raabe, 2015) to enable correlative TEM/APT measurements as described in (Felfer et al., 2012) using FEI Helios Nanolab 600i cross-beam SEM/FIB instruments. All specimens were prepared in a similar way and had comparable initial geometries. The same instrument was used for low kV FIB cleaning using 2 kV acceleration voltage and 40 pA current for 40 s. TEM observations were conducted in bright field scanning TEM mode in a JEOL JEM-2200FS at 200 kV. APT measurements were performed in a Cameca LEAP 3000 HR instrument in voltage mode at 65 K, 0.5% target evaporation rate, 200 kHz and 15% pulse fraction. Here, we conducted low-kV argon ion cleaning in a PECS Model 682 by Gatan at 2 kV, 32 μA, and 5 bar argon pressure. However, also the recently developed triple-beam instruments (FIB/SEM/Ar) might prove useful for this application. The grid holder was tilted to an angle of 35° where it was rotated about its axis at 25 rpm as shown in Figure 5a. The Ar beam in the PECS has its intensity maximum in the center of the measurement chamber.
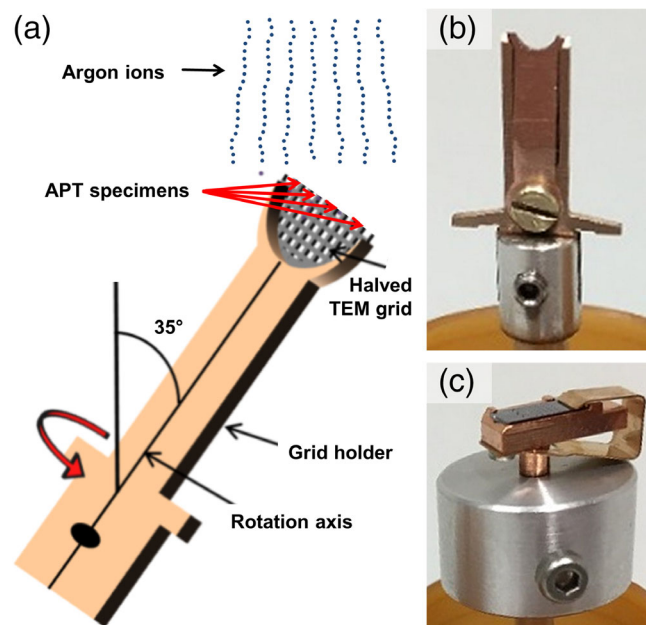

FIGURE 5 APT specimen cleaning using a broad Ar ion beam in a PECS. (a) Schematic setup. The method can be applied to specimens mounted in grid holders (Herbig, Choi, & Raabe, 2015) (b) or on Si coupons (c) using corresponding adapters [Color figure can be viewed at wileyonlinelibrary.com]

The height of adapter pieces must be adjusted correspondingly for maximum efficiency when sputtering the specimen-containing top of the inclined holders. A particularly short adapter piece had to be used for the long grid holders used for the experiments described in this work (see Figure 5b). However, this method is also applicable to clean specimens mounted on Si coupons in commercial clip holders when using a modified adapter (Figure 5c). This way, also the standard APT specimens can be cleaned in an efficient way after oxidation or after conducting TKD.

Figure 6 shows the effect of Ar ion cleaning on an oxidized and hydrocarbon-contaminated specimen. The specimen is shown before and after ion cleaning in Figure 6a,b, respectively. Five minutes of cleaning are sufficient to completely remove the detrimental layer from the surface for all specimens present on the grid at once. According to SRIM simulations (Ziegler, Ziegler, & Biersack, 2010) the exposure of Fe to 2 kV Ar ions results in a beam-damaged layer of about 3 nm thickness (Sato et al., 2020) which is acceptable also for high resolution TEM investigations. For the investigation of materials which are more sensitive to beam damage than steels, such as semi-conductors, the Ar ion beam acceleration voltage can be further reduced. Sputtering of GaAs with a 200 eV Ar beam at an angle of 30° was reported to result in a beam-damaged layer of 2.6 nm thickness (Matsutani, Iwamoto, Nagatomi, Kimura, & Takai, 2001). The argon ion cleaning procedure was conducted at various tilt angles. Working with a nanocrystalline material where the microstructure is clearly visible in TEM (Figure 6a,b) enabled to quantify how much material was removed from which location of the specimen. A tilt angle of 35° was found optimal for a 1:1 ratio between material removal from the specimen apex and shank, leading for steels to about 8 nm material removal evenly from all specimen sides in 5 min of cleaning using the above-mentioned conditions. The specimen

depicted in Figure 6b was subsequently measured by APT as shown in Figure 6c. All APT voltage curves measured by EM and cleaned in the above-described way showed a similar behavior. No abrupt changes in the specimen voltage indicating microfractures or sudden bursts of detection events were observed although the measurement
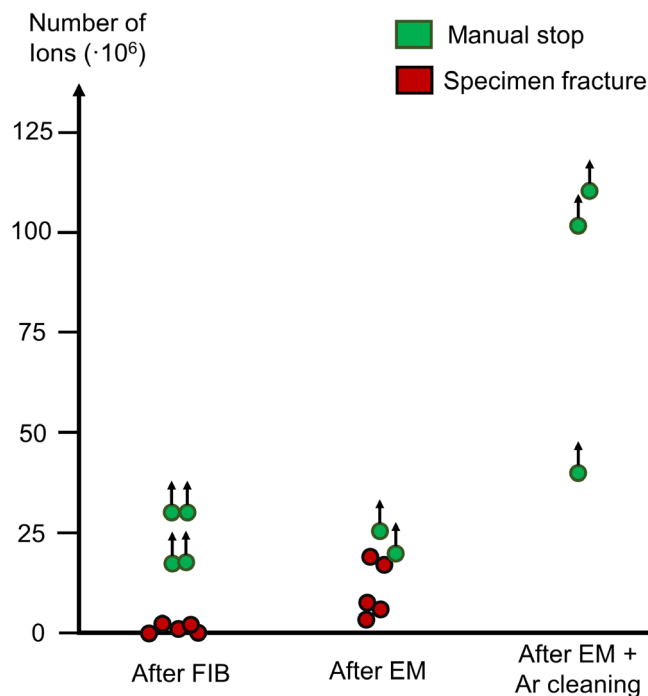

FIGURE 7 Comparison of APT measurement yield of specimens measured directly after FIB preparation, after electron microscopy (EM) and after EM followed by Ar ion cleaning [Color figure can be viewed at wileyonlinelibrary.com]
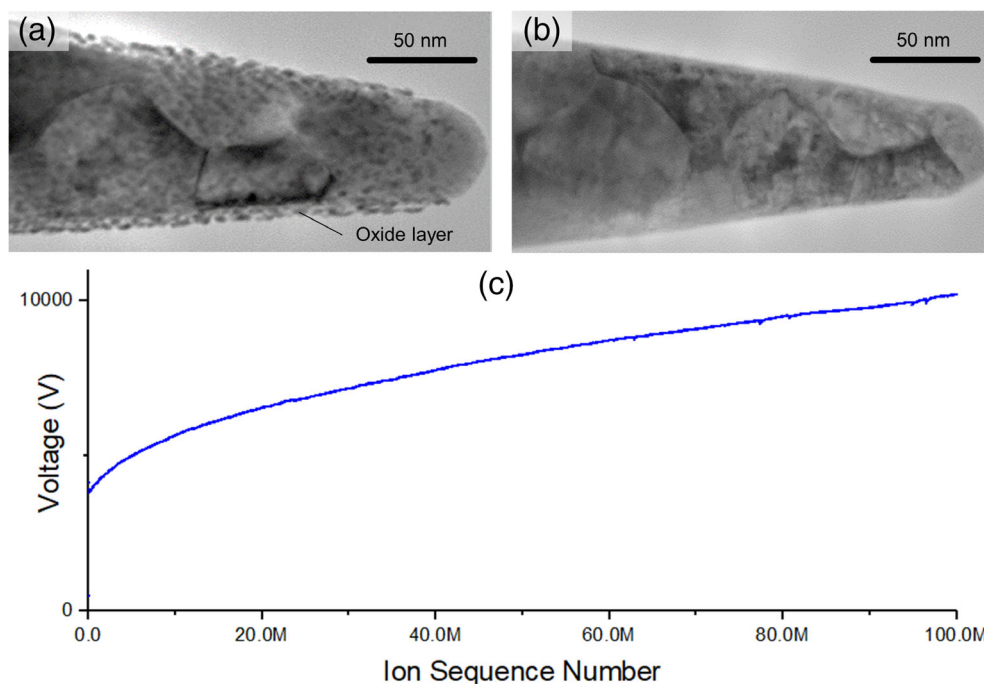

FIGURE 6 (a) Oxidized and hydrocarbon-contaminated APT specimen after EM. (b) Same specimen after Ar ion cleaning. Oxide and hydrocarbon layers are homogenously removed by the treatment. (c) APT voltage curve of the specimen shown in (b). The APT measurement quality is equally smooth as for specimens not investigated by EM (compare Figure 1) [Color figure can be viewed at wileyonlinelibrary.com]

was extremely long considering that it was conducted in a LEAP 3000 HR system with 38% detection efficiency: after collecting 102 million ions in 26 hr the measurement had to be switched off manually due to the lack of experimental time. The comparison between Figure 1b and Figure 6c shows that Ar ion cleaning restores the APT measurement yield and quality of specimens measured by EM to a level at least as good as compared to specimens directly measured by APT after preparation.

However, Figure 7 indicates that this improvement might even go beyond that. In this plot, red dots mark specimens that fractured during the APT experiment, while green dots with an arrow mark those that were interrupted manually as enough ions were collected or due to the lack of measurement time, that is, those runs could have continued. For specimens measured directly after FIB preparation about 55% fracture below 20 million ions. This percentage raises to about 70% after EM. The low number of very short runs after EM as compared to after FIB reflects the fact that in EM specimens were inspected for preparation damage and only undamaged specimens were measured by APT. Without this step, the difference in measurement yield between specimens measured directly after FIB preparation compared to after EM would be even more prominent. After Ar ion cleaning no specimen fracture was observed anymore and all specimens ran smoothly for more than 40 million ions. In an attempt to provoke failure during APT, two specimens were run for more than 24 hr and 100 million atoms each. However, no specimen failure occurred also for these extremely long run times and finally the measurements had to be stopped manually due to the lack of experimental time. This might mean, that Ar ion cleaning might not only restore the measurement yield of specimens pre-characterized by EM to the level of FIB-prepared specimens but even beyond that. Considering the high costs involved in APT measurements as well as in FIB-based specimen preparation and the comparably low costs for an Ar-ions cleaning device as used here this possibility sounds appealing. However, this point requires further statistical clarification.

3 | CONCLUSIONS

Hydrocarbon contamination created by EM and oxide layers created by sample storage and transport compromise the APT measurement yield and quality. Plasma cleaning efficiently removes hydrocarbon contamination but oxidizes the specimen. Specimen cleaning by low-kV FIB milling is time-consuming, costly and removes primarily the tip apex while the detrimental layers on the shank remain. Ar ion cleaning using a PECS, normally used to clean and coat SEM specimens, is ideally suited for gentle, user-friendly, reproducible, and automated removal of hydrocarbon contamination and oxides from APT specimens. The broad ion beam geometry and the possibility to tilt and rotate the specimens about their axes allows homogenous material removal from all sides. Beam operation at low voltage minimizes beam damage. The use of Ar ions minimizes chemical reactions between beam and specimen surface. The method is efficient as all APT specimens present on the grid or clip holder can be cleaned at once in

a five-minute treatment. A tendency is observed that specimens after EM followed by Ar ion cleaning have an even higher APT measurement yield than those directly measured after FIB preparation. This indicates that Ar ion cleaning might be beneficial in general for all APT specimens. However, in particular for specimens pre-characterized by EM, being more precious than conventional ones, Ar ion cleaning should be conducted.

ORCID

Michael Herbig 🄳 https://orcid.org/0000-0001-9561-6139

REFERENCES

Babinsky, K., De Kloe, R., Clemens, H., & Primig, S. (2014). A novel approach for site-specific atom probe specimen preparation by focused ion beam and transmission electron backscatter diffraction. *Ultramicroscopy*, *144*, 9–18. https://doi.org/10.1016/j.ultramic.2014.04.003

Felfer, P. J., Alam, T., Ringer, S. P., & Cairney, J. M. (2012). A reproducible method for damage-free site-specific preparation of atom probe tips from interfaces. *Microscopy Research and Technique*, *75*(4), 484–491. https://doi.org/10.1002/jemt.21081

Gault, B., Menand, A., de Geuser, F., Deconihout, B., & Danoix, R. (2006). Investigation of an oxide layer by femtosecond-laser-assisted atom probe tomography. *Applied Physics Letters*, *88*(11). Artn 114101. https://doi.org/10.1063/1.2186394

Haley, D., Petersen, T., Ringer, S. P., & Smith, G. D. W. (2011). Atom probe trajectory mapping using experimental tip shape measurements. *Journal of Microscopy*, *244*(2), 170–180. https://doi.org/10.1111/j.1365-2818.2011.03522.x

Herbig, M. (2018). Spatially correlated electron microscopy and atom probe tomography: Current possibilities and future perspectives. *Scripta Materialia*, *148*, 98–105. https://doi.org/10.1016/j.scriptamat.2017.03.017

Herbig, M., Choi, P., & Raabe, D. (2015). Combining structural and chemical information at the nanometer scale by correlative transmission electron microscopy and atom probe tomography. *Ultramicroscopy*, *153*, 32–39. https://doi.org/10.1016/j.ultramic.2015.02.003

Herbig, M., Kuzmina, M., Haase, C., Marceau, R. K. W., Gutierrez-Urrutia, I., Haley, D., … Raabe, D. (2015). Grain boundary segregation in Fe–Mn–C twinning-induced plasticity steels studied by correlative electron backscatter diffraction and atom probe tomography. *Acta Materialia*, *83*, 37–47. https://doi.org/10.1016/j.actamat.2014.09.041

Herbig, M., Raabe, D., Li, Y. J., Choi, P., Zaefferer, S., & Goto, S. (2014). Atomic-scale quantification of grain boundary segregation in Nanocrystalline material. *Physical Review Letters*, *112*(12), 126103. https://doi.org/10.1103/Physrevlett.112.126103

Hettler, S., Dries, M., Hermann, P., Obermair, M., Gerthsen, D., & Malac, M. (2017). Carbon contamination in scanning transmission electron microscopy and its impact on phase-plate applications. *Micron*, *96*, 38–47. https://doi.org/10.1016/j.micron.2017.02.002

Isabell, T. C., Fischione, P. E., O'Keefe, C., Guruz, M. U., & Dravid, V. P. (1999). Plasma cleaning and its applications for electron microscopy. *Microscopy and Microanalysis*, *5*(2), 126–135. https://doi.org/10.1017/S1431927699000094

Krakauer, B. W., Hu, J. G., Kuo, S. M., Mallick, R. L., Seki, A., Seidman, D. N., … Loyd, R. J. (1990). A system for systematically preparing atom-probe field-ion-microscope specimens for the study

of internal interfaces. *Review of Scientific Instruments*, *61*(11), 3390–3398. https://doi.org/10.1063/1.1141590

Kuzmina, M., Herbig, M., Ponge, D., Sandlobes, S., & Raabe, D. (2015). Linear complexions: Confined chemical and structural states at dislocations. *Science*, *349*(6252), 1080–1083. https://doi.org/10.1126/science.aab2633

Liebscher, C. H., Stoffers, A., Alam, M., Lymperakis, L., Cojocaru-Miredin, O., Gault, B., ... Raabe, D. (2018). Strain-induced asymmetric line segregation at faceted Si grain boundaries. *Physical Review Letters*, *121*(1), 015702. https://doi.org/10.1103/PhysRevLett.121.015702

Loberg, B., & Norden, H. (1969). Observations of field-evaporation end form of tungsten. *Arkiv for Fysik*, *39*(4), 383–395.

Love, G., Scott, V. D., Dennis, N. M. T., & Laurenson, L. (1981). Sources of contamination in Electron-optical equipment. *Scanning*, *4*(1), 32–39. https://doi.org/10.1002/sca.4950040105

Matsutani, T., Iwamoto, K., Nagatomi, T., Kimura, Y., & Takai, Y. (2001). Flattening of surface by sputter-etching with low-energy ions. *Japanese Journal of Applied Physics Part 2-Letters*, *40*(5a), L481–L483. https://doi.org/10.1143/Jjap.40.L481

Rigutti, L., Blum, I., Shinde, D., Hernandez-Maldonado, D., Lefebvre, W., Houard, J., ... Deconihout, B. (2014). Correlation of micro-photoluminescence spectroscopy, scanning transmission Electron microscopy, and atom probe tomography on a single Nano-object containing an InGaN/GaN multiquantum well system. *Nano Letters*, *14*(1), 107–114. https://doi.org/10.1021/Nl4034768

Sato, T., Aizawa, Y., Matsumoto, H., Kiyohara, M., Kamiya, C., & Von Cube, F. (2020). Low damage lamella preparation of metallic materials by FIB processing with low acceleration voltage and a low incident angle Ar ion milling finish. *Journal of Microscopy*, *279*, 234–241. https://doi.org/10.1111/jmi.12878

Stoffers, A., Cojocaru-Miredin, O., Seifert, W., Zaefferer, S., Riepe, S., & Raabe, D. (2015). Grain boundary segregation in multicrystalline silicon: Correlative characterization by EBSD, EBIC, and atom probe tomography. *Progress in Photovoltaics*, *23*(12), 1742–1753. https://doi.org/10.1002/pip.2614

Thompson, K., Gorman, B., Larson, D. J., Leer, B. v., & Hong, L. (2006). Minimization of Ga induced FIB damage using low energy clean-up. *Microscopy and Microanalysis*, *12*(s02), 1736–1737.

Toji, Y., Matsuda, H., Herbig, M., Choi, P. P., & Raabe, D. (2014). Atomic-scale analysis of carbon partitioning between martensite and austenite by atom probe tomography and correlative transmission electron microscopy. *Acta Materialia*, *65*, 215–228. https://doi.org/10.1016/j.actamat.2013.10.064

Zhou, X. Y., Yu, X. X., Kaub, T., Martens, R. L., & Thompson, G. B. (2016). Grain boundary specific segregation in nanocrystalline Fe(Cr). *Scientific Reports*, *6*, 34642. https://doi.org/10.1038/srep34642

Ziegler, J. F., Ziegler, M. D., & Biersack, J. P. (2010). SRIM - the stopping and range of ions in matter (2010). *Nuclear Instruments & Methods in Physics Research Section B-Beam Interactions with Materials and Atoms*, *268*(11–12), 1818–1823. https://doi.org/10.1016/j.nimb.2010.02.091